ELSEVIER

Boundary-layer regime in a vertical porous layer with anisotropic permeability and boundary effects

G. Degan and P. Vasseur
Department of Mechanical Engineering, Ecole Polytechnique, University of Montreal, Montreal, PQ, Canada

In this paper, natural convection heat transfer in a vertical porous layer is studied both analytically and numerically. A constant heat flux is applied for heating and cooling the long side walls of the rectangular cavity, while the other two walls are insulated. The porous medium is assumed to be hydrodynamically anisotropic with its principal axes oriented in a direction that is oblique to the gravity vector. In the formulation of the problem, use is made of the Brinkman-extended Darcy model which allows the no-slip boundary condition on a solid wall, to be satisfied. The governing equations are solved analytically, under the boundary-layer approximations, using the modified Oseen technique. The effects of varying the Rayleigh and Darcy numbers, the anisotropic permeability ratio, and the orientation angle of the principle axes on the flow and heat transfer are investigated. A numerical study of the same phenomenon, obtained by solving the complete system of governing equations, is also conducted. Results are reported in the range $500 \le R \le 1000$, $10^{-7} \le Da \le 10^{3}$, $0.25 \le K^{*} \le 4$, $0° \le \theta \le 90°$, and $A = 1$ and 4. Good agreement is found between the analytical prediction and the numerical solution.

Keywords: natural convection; anisotropic porous medium

Introduction

Convection heat transfer in porous media is of fundamental importance in such technologies as geothermal exploitation, oil recovery, and radioactive waste management. It is also important to geophysics and environmental sciences. Much of this activity, both numerical and experimental, has been summarized by Nield and Bejan (1992). A review of the literature shows that most previous studies on heat transfer in porous media considered the isotropic situation; whereas, in several applications, the porous materials are anisotropic. Despite this, natural convection in such anisotropic porous media has received relatively little attention.

Thermal convection in a porous medium with anisotropic permeability was first considered by Castinel and Combarnous (1974), who conducted an experimental and theoretical investigation in a horizontal layer heated from below. The critical Rayleigh number for the onset of convection was predicted by these authors. Their results were extended by Epherre (1975) and Kvernvold and Tyvand (1979) who considered a more general type of anistropy. The effects of anisotropy on the steady flow patterns at slightly supercritical Rayleigh numbers were discussed by Nilsen and Storesletten (1990). The stability of these flow patterns were examined against two-dimensional (2-D) perturbations using a weakly nonlinear theory. Convection attributable to side-heating in a vertical cavity has also been considered by several authors. For example, the case of a square cavity with homogeneous media that is both thermally and hydrodynamically anisotropic has been investigated analytically by Kimura et al. (1993) and numerically by Ni and Beckermann (1991). The effect of both anisotropy of permeability and thermal conductivity on the overall Nusselt number was found to be equally significant.

A few studies have also been concerned with the case when the principal axes of anisotropy of the porous structure are inclined with respect to the gravity force. For this situation, the onset of motion in a porous layer heated from below was predicted by Tyvand and Storesletten (1991) and Zhang et al. (1993). It was demonstrated that the influence of the anisotropy orientation considerably modifies the stability limit. Convective heat transfer in a vertical cavity heated from the side with various thermal boundary conditions has been investigated by Zhang (1993), Degan et al. (1995), and Degan and Vasseur (1996). It was demonstrated that the heat transfer was maximum when the principal axis with higher permeability is parallel to the vertical direction, and minimum when it is perpendicular. A numerical study of natural convection taking place between horizontal concentric cylinders heated isothermally has been performed by Aboubi et al. (1995). Results indicate that for an arbitrary inclination of the principal axes, which differs from the horizontal or the vertical direction, a net circulating flow occurs around the annulus, with the maximum value reached when the principal axes are approximately at 45° with respect to the vertical direction.

Address reprint requests to Dr. P. Vasseur, Dept. of Mechanical Engineering, Ecole Polytechnique, University of Montreal, C. P. 6079, Succ-Centre-Ville, Montreal, PQ II3C 3A7, Canada.

Received 3 April 1996; accepted 23 September 1996

Int. J. Heat and Fluid Flow 18: 334–343, 1997

655 Avenue of the Americas, New York, NY 10010

0142-727X/97/$17.00
PII S0142-727X(97)00011-8

In all the studies cited, the porous media have been modeled according the Darcy's law. The main advantage of the Darcy flow model is that it linearizes the momentum equation, thus removing a considerable amount of difficulty in solving the governing equations. It has been demonstrated in the past by Cheng (1978), Chan et al. (1970), Tong and Subramanian (1985), and Vasseur and Robillard (1987), among others, that Darcy's law is, indeed, a good approximation for low-porosity media; i.e., when the Darcy number Da, based on the height of the porous medium is less than approximately 10^{-3}. However, for higher values of Da, Darcy's model may incorrectly overpredict the heat transfer and flow rate, because it cannot account for the no-slip boundary condition on rigid boundaries. To consider the boundary effect, which may become important in porous media with high porosities, Brinkman's extension of Darcy's law should be used.

The purpose of the present work is to study the boundary effect in a vertical cavity filled with a porous medium anisotropic in permeability. A constant heat flux is applied on the vertical side walls, while the top and bottom walls are adiabatic. The problem is formulated in terms of the Brinkman-extended Darcy model. The porous medium is anisotropic in permeability with its principal axes oriented in a direction oblique to the gravity vector. On the basis of a modified Oseen linearization method, a closed-form solution is obtained for the temperature and velocity distributions in the boundary-layer flow regime. The full governing equations are solved numerically, using a finite-difference procedure, to assess the validity of the analytical results. Effects of various parameters, such as the Rayleigh number R, the Darcy number Da, the permeability ratio K^*, and the rotation angle θ of the principal axes are analyzed.

Mathematical formulation

The physical situation and coordinate system are depicted in Figure 1. The vertical rectangular enclosure is of height H' and thickness L'. The two end walls are insulated while a uniform heat flux q' is applied along both side walls. The thermophysical properties of the fluid are assumed constant, except for the density in the buoyancy term in the momentum equations. The porous medium is anisotropic, the permeabilities along the two principal axes of the porous matrix being denoted by K_1 and K_2. The anisotropy of the porous medium is then characterized by the permeabilities K_1 and K_2 and the orientation angle θ, defined as the angle between the horizontal direction and the principal axis with permeability K_2.

Under the above approximations, the equations governing the conservation of mass, momentum, and energy can be written as follows.

$$\nabla \cdot \mathbf{V}' = 0 \tag{1}$$

$$\mathbf{V}' = \frac{\bar{\bar{K}}'}{\mu}(-\nabla p' + \varrho \mathbf{g} + \mu_{\text{eff}} \nabla^2 \mathbf{V}') \tag{2}$$

$$(\varrho c)_p \frac{\partial T'}{\partial t'} + (\varrho c)_f \nabla \cdot (\mathbf{V}' T') = k \nabla^2 T' \tag{3}$$

where $\mathbf{V}'$ is the superficial flow velocity, T' temperature, p' pressure, ϱ density, $\mathbf{g}$ gravitational acceleration, t' time, $(\varrho c)_p$ and $(\varrho c)_f$ heat capacities of the saturated porous medium and the fluid, respectively, μ dynamic viscosity, μ_{eff} apparent dynamic viscosity for Brinkman's model, and k thermal conductiv-

Notation

A	aspect ratio of the cavity, H'/L'
C	vertical temperature gradient in the core of the cavity, $\Delta T^*/A$
a, b, c	constants, Equation 7
Da	Darcy number, K_1/L'^2
g	gravitational acceleration
H'	height of the cavity
k	thermal conductivity of the saturated porous medium
$\bar{\bar{K}}'$	flow permeability tensor, defined in Equation 4
K_1, K_2	flow permeability along the principal axes
K^*	permeability ratio, K_1/K_2
L'	thickness of the cavity
Nu	Nusselt number, Equation 11
p'	pressure
q'	uniform flux of heat (per unit area)
R	Rayleigh number for porous media, $K_{1G}\beta L'^2 q'/k\alpha\nu$
Ra	Raleigh number of a fluid, R/Da
t'	time
T'_o	reference temperature at the geometric center of the cavity
T	dimensionless temperature, $(T' - T'_o)/\Delta T'$
ΔT	dimensionless wall-to-wall temperature difference at $x = \text{const}$
ΔT^*	temperature difference between horizontal boundaries
$\Delta T'$	characteristic temperature difference, $q'L'/k$
V'	seepage velocity
u, v	dimensionless velocities in x- and y-directions, $(u', v')L'/\alpha$
x, y	dimensionless cartesian coordinates $(x', y')/L'$

Greek

α	thermal diffusivity
β	coefficient of thermal expansion of the fluid
δ	dimensionless thickness of the horizontal boundary layer, δ'/L'
δT	temperature difference between vertical boundaries
θ	inclination of the principal axes
μ	dynamic viscosity of the fluid
μ_{eff}	apparent dynamic viscosity for Brinkman's model
λ	relative viscosity, μ_{eff}/μ
ν	kinematic viscosity of the fluid
ϱ	density of the fluid
$(\varrho c)_f$	heat capacity of the fluid
$(\varrho c)_p$	heat capacity of the saturated porous medium
σ	heat capacity ratio, $(\varrho c)_p/(\varrho c)_f$
ψ	dimensionless stream function, ψ'/α

Superscript

'	dimensional quantities

Subscripts

o	refers to the center of the cavity
∞	refers to the core region
max	maximum value

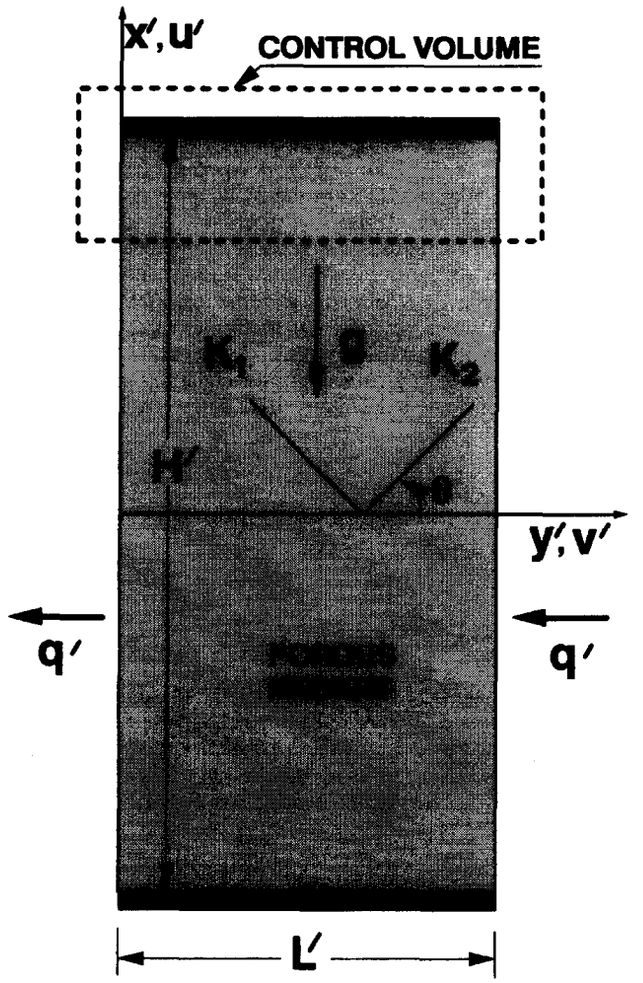

Figure 1 Physical situation and coordinate system

ity. The second-order permeability tensor $\bar{\bar{K}}'$ is defined as

$$\bar{\bar{K}}' = \begin{bmatrix} K_1\cos^2\theta + K_2\sin^2\theta & (K_1 - K_2)\sin\theta\cos\theta \\ (K_1 - K_2)\sin\theta\cos\theta & K_2\cos^2\theta + K_1\sin^2\theta \end{bmatrix} \tag{4}$$

Introducing the Boussinesq approximation, eliminating the pressure term in the momentum equation in the usual way, and taking $L', \alpha/L'$ [where $\alpha = k/(\varrho c)_f$], $\Delta T' = q'L'/k$ and $L'^2\sigma/\alpha[\sigma = (\varrho c)_p/(\varrho c)_f]$ as respective dimensional scales for length, velocity, temperature, and time, the governing equations may be written in nondimensional form as

$$a\frac{\partial^2\psi}{\partial y^2} + b\frac{\partial^2\psi}{\partial x\,\partial y} + c\frac{\partial^2\psi}{\partial x^2} = \lambda\,\mathrm{Da}\,\nabla^4\psi + \mathrm{R}\frac{\partial T}{\partial y} \tag{5}$$

$$\frac{\partial T}{\partial t} + \frac{\partial\psi}{\partial y}\frac{\partial T}{\partial x} - \frac{\partial\psi}{\partial x}\frac{\partial T}{\partial y} = \nabla^2 T \tag{6}$$

where

$$\left.\begin{aligned} a &= \cos^2\theta + K^*\sin^2\theta \\ b &= 2(K^* - 1)\sin\theta\cos\theta \\ c &= \sin^2\theta + K^*\cos^2\theta \end{aligned}\right\} \tag{7}$$

In the above equations, $\mathrm{R} = K_{1G}\beta q' L'^2/k\alpha\nu$, is the Rayleigh number based on permeability K_1, $K^* = K_1/K_2$ the permeability ratio, $\lambda = \mu_{\mathrm{eff}}/\mu$ the relative viscosity, $\mathrm{Da} = K_1/L'^2$ the Darcy number, and ψ the stream function related to the velocity components by

$$u = \frac{\partial\psi}{\partial y}, \qquad v = -\frac{\partial\psi}{\partial x} \tag{8}$$

so that the continuity Equation 1 is automatically satisfied.

For an isotropic porous medium ($K^* = 1$), the set of Equations 5–7 reduces to the usual Brinkman-extended Darcy model used in the past by many authors (see e.g. Tong and Subramanian 1985).

The boundary conditions are given in dimensionless form as

$$\text{at } x = \pm A/2: \qquad \psi = \frac{\partial\psi}{\partial x} = 0, \qquad \frac{\partial T}{\partial x} = 0 \tag{9}$$

$$\text{at } y = 0, 1: \qquad \psi = \frac{\partial\psi}{\partial y} = 0, \qquad \frac{\partial T}{\partial y} = 1 \tag{10}$$

where $A = H'/L'$ is the cavity aspect ratio.

From the dimensionless Equations 5–10, it is seen that the present problem is governed by six dimensionless parameters; namely R, Da, λ, θ, K^*, and A. However, in the present study, the value of μ_{eff} in Brinkman's extension is taken, as a first approximation, equal to μ (i.e., $\lambda = 1$).

The heat transfer across the system can be expressed in term of a Nusselt number at $y = 0$, defined as

$$\mathrm{Nu} = \left(\frac{q'}{\Delta T'}\right)\frac{L'}{k} = \frac{1}{\Delta T} \tag{11}$$

where ΔT is the actual wall-to-wall temperature difference which, because of the thermal boundary conditions considered here, will be demonstrated to be independent of altitude x.

Numerical solution

The solution of governing Equations 5–8 under boundary conditions (Equations 9–10) was obtained using a standard finite-difference numerical method. The first-order derivatives were approximated by central differences, and second-order approximations were used for the derivatives in the boundary conditions. The temperature field was first found by solving Equation 6 using an alternating-direction-implicit procedure (ADI) and assuming known initial ψ and T fields. Once the temperature had been determined, Equation 5 was solved using a successive over-relaxation method (SOR). The ψ values so obtained were used in Equation 6 together with the more recently calculated temperature field to obtain new values for the temperature. The iterative cycle was repeated until a convergence criterion of 0.05% was satisfied. The heat transfer through each plane $y = cte$ was evaluated at each grid location $0 \le y \le 1$ and compared with the input at $y = 1$. Such an energy balance was satisfied to within 0.1% for most of the results reported here.

For the present work, uniform mesh sizes have been used for both x- and y-directions. Based on the several trial cases, a suitable grid field of 50×50 was selected for the present calculations. In the cases where the Rayleigh number was large, the grid fineness was improved up to 50×80. Typical values of the time-steps range from 5×10^{-5} to 10^{-3}. The CPU time required to reach steady state was approximately from 80 to 480s on an IBM RISC 6000/RS 365 workstation.

Because of the particular thermal boundary conditions considered here, the solution to the present problem is independent of the aspect ratio A of the cavity in the limit of $A \gg 1$. For the case of an isotropic Darcian medium, it has been demonstrated numerically by Vasseur et al. (1987) that this was, indeed, the case when A was approximately equal to or greater than 2. Other tests have been performed here, and it was found that Nu converges very fast to an asymptotic value when $A \geq 4$. Therefore, most of the numerical results presented here were obtained for $A = 4$.

Figure 2 illustrates typical streamlines and isothermal patterns, obtained numerically for R = 500, $A = 1$ (i.e., a square cavity) and various values of Da, K^*, and θ. For each map of Figure 2, the increments between adjacent streamlines and isotherms are $\Delta\psi = \psi_{max}/10$ and $\Delta T = (T_{max} - T_{min})/10$ respectively, where ψ_{max} is the maximum value of the stream function and T_{max} and T_{min} the maximum and minimum values of the dimensionless temperature field located at the upper right-hand corner and lower left-hand corner of the cavity, respectively.

Figures 2a, c, and e exemplify the effects of varying the permeability ratio K^* and the angle of the principal axes θ on the flow patterns and isotherms with $Da = 10^{-5}$; i.e., when the Darcy number is relatively small. For this situation, the anisotropic permeability of the porous medium is seen to have a strong influence on the convective flow within the cavity. Thus, for $\theta = 0°$ and $K^* = 10^{-3}$ (Figure 2a), the flow pattern is seen to be strongly channeled along the horizontal boundaries because of the relatively high permeability in that direction. For the same reason, the convective cell for $\theta = 45°$ and $K^* = 10^2$, Figure 2c, is aligned along the diagonal region of the cavity, while for $\theta = 90°$ and $K^* = 10^{-2}$, Figure 2e, the flow is channeled along the thermally active vertical walls. Also, it is observed from the isotherm patterns that the heat transfer across the cavity is promoted as the value of K^* is made smaller. Thus, for $K^* = 10^2$, the heat transfer is almost by pure conduction (Nu = 1.17), as indicated by the nearly vertical isotherms of Figure 2c, while it is relatively high (Nu = 10.78) for $K^* = 10^{-2}$ for which the isotherms of Figure 2e are considerably distorted. This trend

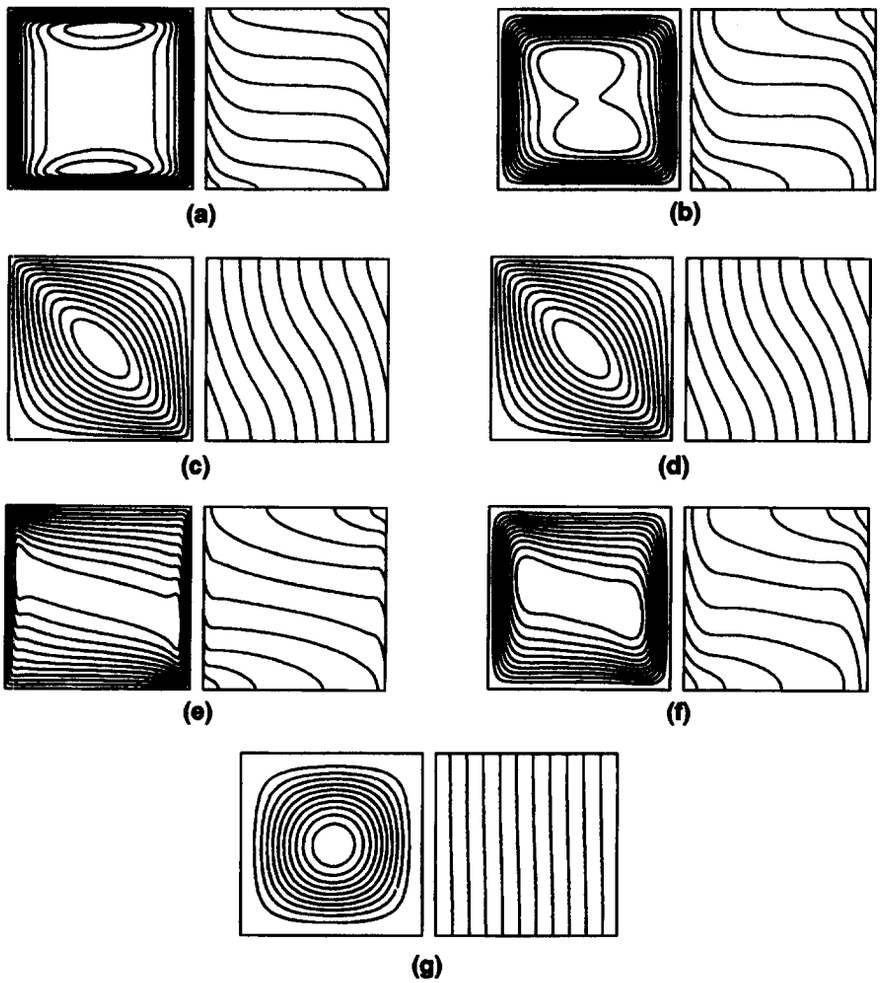

Figure 2 Numerical solutions for the flow and temperature fields, R=500, $A=1$ and: a) $Da=10^{-5}$, $\theta=0°$, $K^*=10^{-3}$, $\psi_{max}=4.40$, Nu=5.909, $T_{max}=-T_{min}=0.247$; b) $Da=10^{-3}$, $\theta=0°$, $K^*=10^{-3}$, $\psi_{max}=3.92$, Nu=4.727, $T_{max}=-T_{min}=0.3045$; c) $Da=10^{-5}$, $\theta=45°$, $K^*=10^2$, $\psi_{max}=0.79$, Nu=1.173, $T_{max}=-T_{min}=0.576$; d) $Da=10^{-3}$, $\theta=45°$, $K^*=10^2$, $\psi_{max}=0.785$, Nu=1.170, $T_{max}=-T_{min}=0.5759$; e) $Da=10^{-5}$, $\theta=90°$, $K^*=10^{-2}$, $\psi_{max}=4.77$, Nu=10.781, $T_{max}=-T_{min}=0.2613$; f) $Da=10^{-3}$, $\theta=90°$, $K^*=10^{-2}$, $\psi_{max}=4.175$, Nu=5.414, $T_{max}=-T_{min}=0.3041$; and g) Da=10, $\psi_{max}=0.0528$, Nu=1.00, $T_{max}=-T_{min}=0.5068$;

follows from the fact that for a fixed value of R (i.e., K_1) a decrease in K^* involves an increase in the permeability K_2, resulting in a stronger flow, thus promoting the heat transfer.

The results obtained above for $Da = 10^{-5}$ are qualitatively similar to those reported by Ni and Beckermann (1991) and Degan et al. (1995; 1996) on the basis of Darcy's law; i.e., for low-porosity media. This result is expected, because when Da is small enough, the viscous terms, which are responsible for the boundary effects, are negligibly small, and Darcy's law correctly describes the flow behavior. However, for porous media with high porosities, such as foam metals and fibrous media, the boundary effects may become important, and Brinkman's extension of Darcy's law must be used. Hence, upon increasing the Darcy number from $Da = 10^{-5}$ to $Da = 10^{-3}$, the resulting flow patterns, Figures 2b, d, and f, are observed to be considerably modified (expected for $K^* = 10^2$, Figures 2c and d, for which the convection is so weak that the effect of Da is negligible). In particular, the streamlines are seen to be more sparsely spaced near the solid boundaries as the value of Da increases. This is expected, because the viscous term (Brinkman) becomes more important and slows down the fluid in the neighborhood of the walls. Also, the effects of varying the anisotropic properties of the porous medium are observed to become less significant. This follows from the fact that, as the Darcy number is increased, the boundary frictional resistance is enhanced and adds to the bulk frictional drag induced by the solid matrix to slow the convection motion. As a result, the influence of the anisotropic permeability of the porous medium becomes gradually less important. Thus, when $Da = 10$, the flow pattern illustrated in Figure 2g corresponds approximately to that of a pure fluid situation for which the anisotropy of the porous medium is irrelevant.

Approximate analytical solution

In this section, an approximate analytical solution is presented for the case of convection at large Rayleigh numbers. When R is large enough, the flow will have a boundary-layer-core structure consisting of a thermally stratified core region and two vertical boundary layers. For this situation, the orders of magnitude of the quantities of interest involved in the problem can be predicted on scaling grounds. Also, as is demonstrated, it is possible to derive an analytical solution to the steady-state problem valid for a large domain of parameter values.

Scale analysis

In the boundary-layer regime, most of the fluid motion is confined to a thin vertical boundary layer of dimensionless thickness $\delta = \delta'/L'$. Let δu and δT be the velocity and temperature changes across this layer and ΔT^* the temperature difference between the horizontal boundaries. The two temperature scales δT and ΔT^*, although interrelated, are quite different and must be treated appropriately in evaluating the conduction and convection terms.

As the heat flux is imposed along the vertical boundaries, we must have

$$\frac{\delta T}{\delta y} \sim 1 \tag{12}$$

while the equation governing the conservation of energy requires that

$$\delta u C \sim \frac{\delta T}{\delta y^2} \tag{13}$$

where $C = \Delta T^*/A$ is the vertical temperature gradient in the core of the cavity.

The momemtum Equation 5 indicates that, in the general case, the buoyancy forces are related in so complicated a way with the inertia and the viscous terms that it would not allow for estimations of the order of magnitude of the stream function by scale analysis. However, for the two limiting cases of low-porosity media ($Da \to 0$) and high-porosity media ($Da \to \infty$), order-of-magnitude estimates can be derived on scaling grounds.

Da ≪ 1: the low porosity media limit. For this situation, as demonstrated by the numerical results of Figure 2, the anisotropy effects (i.e., the terms on the left-hand side of Equation 5) are predominant. A balance between those terms and the buoyancy term requires that

$$R\frac{\delta T}{\delta y} \sim a\frac{\delta u}{\delta y} \tag{14}$$

Moreover, the temperature gradient C can be determined, by using an energy flux integral at any x-section (see, e.g., Bejan 1983), as

$$C \sim \delta u\, \delta T\, \delta y \tag{15}$$

Solving Equations 12–15, it is readily found that

$$\delta u \sim \left(\frac{R}{a}\right)^{3/5}, \qquad \delta y = \delta T \sim \left(\frac{R}{a}\right)^{-2/5}, \qquad C \sim \left(\frac{R}{a}\right)^{-1/5} \tag{16}$$

while the Nusselt number, Equation 11, is given by

$$Nu \sim R^{2/5} a^{-2/5} \tag{17}$$

Similar results have been obtained by Degan et al. (1995) while considering the present problem on the basis of the Darcy model.

Da ≫ 1: the high porosity media limit. For this situation, a balance between the buoyancy and the viscous terms in Equation 5 requires

$$R\frac{\delta T}{\delta y} \sim Da\frac{\delta u}{\delta y^3} \tag{18}$$

so that Equations 12, 13, 15, and 18 yield

$$\left.\begin{array}{ll} \delta u \sim Ra^{3/9} & \delta y = \delta T \sim Ra^{-2/9} \\ C \sim Ra^{-1/9} & Nu \sim Ra^{2/9} \end{array}\right\} \tag{19}$$

where $Ra = R\ Da^{-1}$ is the Rayleigh number for a pure fluid medium.

The above orders of magnitude are in agreement with the analytical solution predicted by Kimura and Bejan (1984) for the case of a vertical fluid cavity heated from the sides by constant heat fluxes.

Boundary-layer approximation

In this section, expressions for the velocity and temperature fields, valid in the boundary-layer regime ($R \to \infty$), are derived. Making the usual boundary-layer simplifications, the approxi-

mate forms of Equations 1, 5, and 6 can be obtained as

$$\frac{\partial u}{\partial x}+\frac{\partial v}{\partial y}=0 \tag{20}$$

$$a\frac{\partial u}{\partial y}=\mathrm{Da}\frac{\partial^3 u}{\partial y^3}+\mathrm{R}\frac{\partial T}{\partial y} \tag{21}$$

$$\frac{\partial^2 T}{\partial y^2}=u\frac{\partial T}{\partial x}+v\frac{\partial T}{\partial y} \tag{22}$$

The corresponding dimensionless boundary conditions for the left boundary layer are

$$y=0: \qquad u=v=0, \qquad \frac{\partial T}{\partial x}=1 \tag{23}$$

$$y\to\infty: \qquad \begin{cases} u\to 0 \\ T\to T_\infty(x) \\ v\to v_\infty(x) \end{cases} \tag{24}$$

where subscript ∞ refers to the conditions in the core of the cavity, outside the boundary layer.

From Equation 5 it is clear that the above boundary-layer approximations are valid only when the second and third terms on the left-hand side can be assumed negligible when compared with the first term. Thus, when the conditions

$$a\frac{\partial^2\psi}{\partial y^2}\gg b\frac{\partial^2\psi}{\partial x\,\partial y} \tag{25}$$

and

$$a\frac{\partial^2\psi}{\partial y^2}\gg c\frac{\partial^2\psi}{\partial x^2} \tag{26}$$

are satisfied.

Upon introducing the orders of magnitude obtained for the low-porosity media limit, for which the effects of varying the anisotropy of the porous matrix are predominant, it is found that the parameters b and c must satisfy the following relationships

$$b\ll Aa^{3/5}\mathrm{R}^{2/5} \tag{27}$$

and

$$c\ll A^2a^{1/5}\mathrm{R}^{4/5} \tag{28}$$

which are not too restrictive, because R, in the boundary-layer regime, is very large.

Equations 20–24 are similar to those derived by Vasseur and Robillard (1987) while considering boundary-layer flows within an isotropic porous cavity ($a=1$). Their solution, based on the modified Oseen method, can be used directly here. From their results, it is readily deduced that the flow and temperature fields for the present problem are given by

$$u=-\frac{32}{BD}\frac{\mathrm{R}}{p}e^{-py/4}\sinh\left(\frac{pD}{4}y\right) \tag{29}$$

$$T=-\frac{4}{D}\mathrm{Da}\,pe^{-py/4}\cosh\left(\frac{pD}{4}y\right)+\frac{au}{2\mathrm{R}}+T_\infty \tag{30}$$

$$\psi_\infty=\frac{64\,\mathrm{Da\,R}}{B^2}, \qquad T_\infty=\frac{x}{\psi_\infty}, \qquad v_\infty=0 \tag{31}$$

where

$$B=(\mathrm{Da}\,p^2-4a)$$

$$D=\sqrt{\left(\frac{8a}{\mathrm{Da}\,p^2}-1\right)} \tag{32}$$

and p is given by the following transcendental equation

$$p=8192\,\mathrm{R}^2\mathrm{Da}^2\frac{(B-8a)}{B^5} \tag{33}$$

From Equation 11, the resulting Nusselt number is given by

$$\mathrm{Nu}=\frac{B}{8\,\mathrm{Da}\,p} \tag{34}$$

Results and discussion

Figures 3a and 3b show, respectively, the vertical velocity and temperature profiles at midheight of the cavity ($x=0$) when R = 500, Da = 10^{-2}, $\alpha=90°$ and various values of K^*. Because

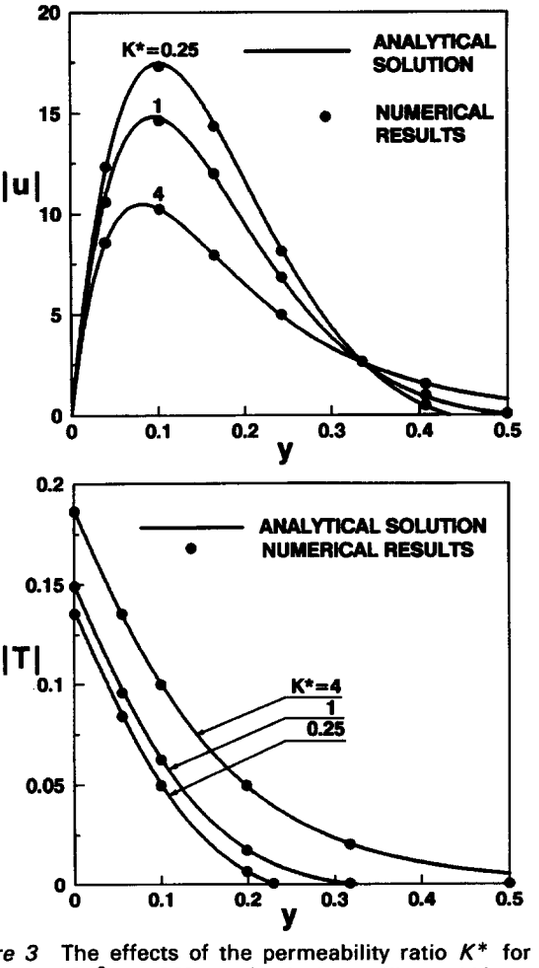

Figure 3 The effects of the permeability ratio K^* for R = 500, Da = 10^{-2}, $\theta=90°$ on: a) velocity profile; and b) temperature profile

the results are antisymmetrical with respect to y, they are presented only for $0 \le y \le 0.5$. The solution of the boundary-layer analysis, represented by solid lines, is seen to agree well with the numerical results depicted by circles. Figure 3a indicates that the velocity at the wall is zero, because, with Brinkman's model, the viscous forces are accounted for and the no-slip boundary condition is satisfied. The velocity increases to a maximum, the position of which depends upon the value of K^*, and then drops back to zero in the core region of the enclosure. In general, Figure 3a indicates that the strength of the convective motion is enhanced, with respect to the case of an isotropic medium ($K^* = 1$), when the permeability ratio K^* is made smaller than one. This is expected, because for a given R (i.e., K_1) a value of K^* smaller than unity, when $\theta = 90°$, corresponds to an increase of the permeability K_2 in the vertical direction, thus promoting the convective circulation within the cavity. Naturally, the reverse trend is achieved when K^* is made larger than 1. The effects of varying K^* on temperature profiles are illustrated in Figure 3b. All the curves have a constant slope at $y = 0$, because a constant heat flux is prescribed on the vertical walls. Also, it is noticed that the temperature on the wall of the cavity, drops as the value of K^* is increased. In the present problem, it should be noted that, contrary to the case of isothermal walls, the effect of varying convection is not to increase the heat flux across the boundaries but rather to decrease the temperature induced within the cavity during this heating process. For this reason, the temperature profiles drop as K^* is made smaller, i.e., as the convection is favoured.

The effects of varying θ, the inclination of the principal axes, on the vertical velocity and temperature profiles are presented in Figures 4a and b for $R = 400$, $Da = 10^{-2}$ and $K^* = 0.25$ (i.e., $K^* < 1$). The results indicate that the strength of the convective motion is maximum when $\theta = 90°$ and minimum when $\theta = 0°$ and, accordingly, the temperature is maximum and minimum when $\theta = 0°$ and 90°, respectively. For ($K^* > 1$), the results (not presented here) show that convection is now maximum when $\theta = 0°$ and minimum when $\theta = 90°$. Thus, the convection motion is maximum when the orientation of the principal axis with higher permeability of the anisotropic porous medium is parallel to the gravity.

The effects of varying the Darcy number Da on the present problem are now discussed. Because it is well known the Brinkman equation reduces to the Darcy situation when $Da \to 0$, and to the pure fluid situation, in the absence of inertia effects, when $Da \to \infty$ these two limits are first discussed.

Da ≫ 1: The Darcy medium situation. When $Da \to 0$ it may be shown that p, Equation 33, reduces to $p \simeq 2[(a/Da)^{1/2} + (R/a)^{2/5}]$. Substituting this result into Equations 29–32 and 34 it is readily found that the velocity and temperature fields and the Nusselt number are given by

$$\psi_\infty = \left(\frac{R}{a}\right)^{1/5}, \qquad T_\infty = \frac{x}{\psi_\infty} \tag{35}$$

$$u = -\left(\frac{R}{a}\right)^{3/5} e^{-(R/a)^{2/5}y}, \qquad T = -\left(\frac{R}{a}\right)^{-2/5} e^{-(R/a)^{2/5}y} + T_\infty \tag{36}$$

$$Nu = \frac{1}{2}\left(\frac{R}{a}\right)^{2/5} \tag{37}$$

which is exactly the behavior predicted by the previous dimensional analysis, as can be seen from Equations 16 and 17.

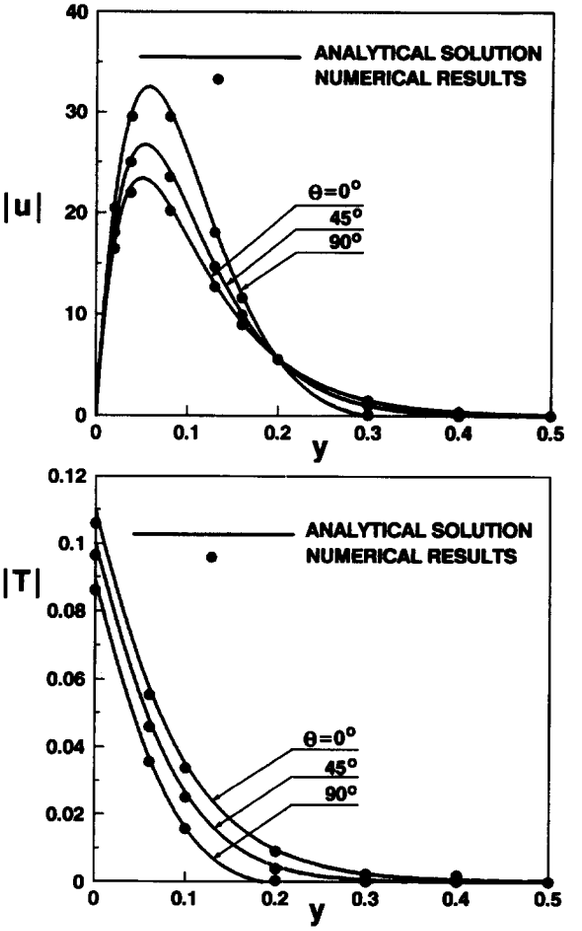

Figure 4 The effects of the inclination angle θ for R=500, $Da = 10^{-2}$, $K^* = 0.25$ on: a) velocity profile; and b) temperature profile

Da ≫ 1: The viscous fluid situation. For this situation, the value of p is approximately given by $p \simeq (8192\ Ra^2)^{1/9}$, and it is found that

$$\psi_\infty = \frac{64\,Ra}{p^4}, \qquad T_\infty = \frac{x}{\psi_\infty} \tag{38}$$

$$u = -\frac{32}{p^3} Ra\, e^{-py/4} \sin\left(\frac{p}{4}y\right),$$

$$T = -\frac{4}{p} e^{-py/4} \cos\left(\frac{p}{4}y\right) + T_\infty \tag{39}$$

$$Nu = \frac{p}{8} \tag{40}$$

in agreement with the predictions of Equation 19.

Upon integrating the velocity profile, Equation 29, over the thickness of the boundary layer, it is found that the resulting flow rate Q is given by $Q = 64\,R\,Da/(Da\,p^2 - 4a)^2$. Similarly, integration of Equations 36 and 39 yields $Q_D = R^{1/5}a^{-1/5}$ for a Darcy medium, and $Q_f = 1.167\ Ra^{1/9}$ for a pure viscous fluid. In Figure 5, the flow rate Q, within the boundary layer, is plotted as a function of Da for the case $R = 500$, $\theta = 45°$ and various values of K^*. The results indicate that, in comparison with the isotropic situation ($K^* = 1$), the flow rate Q is enhanced for $K^* < 1$ and

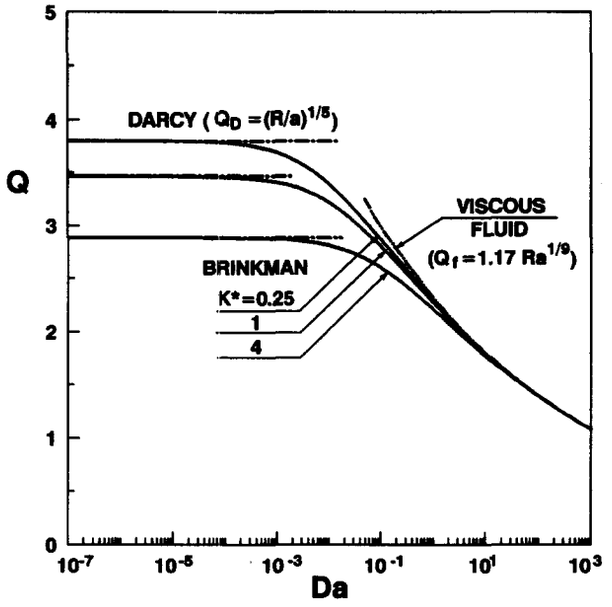

Figure 5 Effect of the Darcy number on the flow rate Q for R=500, θ=45° and various values of K^*

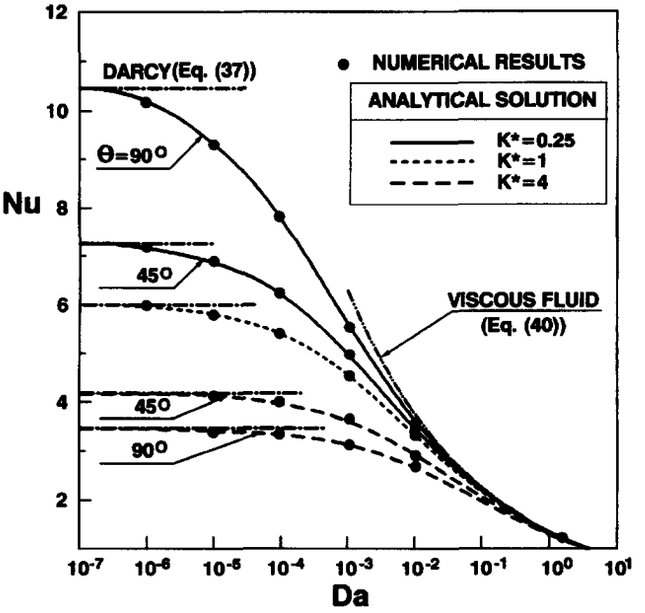

Figure 6 Effect of the Darcy number on Nusselt number for R=500 and various values of K^* and θ

reduced for $K^* > 1$. As discussed previously, this trend follows from the fact that for a fixed value of R (i.e., K_1) an increase (decrease) in K^* corresponds to a decrease (increase) of the permeability K_2, i.e., a weaker (stronger) convective flow. Also, Figure 5 indicates that the flow rates predicted by Darcy's model start to deviate from Brinkman's model at a Darcy number that increases as K^* is made larger. For example, this happens at $Da \simeq 10^{-4}$ when $K^* = 0.25$ and at $Da \simeq 10^{-3}$ when $K^* = 4$. When the Darcy number is made large enough, the results indicate that the curves, for a given value of K^*, tend asymptotically toward the pure fluid situation. The Darcy number required to reach this limit increases as the value of K^* is made larger.

In Figure 6, the Nusselt number, given by Equation 34 is plotted as a function of Da for R = 500 and various values of K^* and θ. A good agreement is observed between the analytical and the numerical results. It is clear from Figure 6 that, when Da is small enough, Nu tends asymptotically toward a constant value that depends on K^* and θ. The limit $Da \to 0$ corresponds to a pure Darcy medium situation for which Nu is given by Equation 37. Thus, for example, Nu = 6 for an isotropic porous medium (K^*, i.e., $a = 1$). In the pure Darcy situation, the effects of the anisotropy of the porous medium on the heat transfer are observed to be significant. Thus, for θ = 90°, the Nusselt number Nu is equal to 10.4 when $K^* = 0.25$ and to 3.5 when $K^* = 4$. When compared with an isotropic porous medium, this represents an increase of about 73% of the heat transfer for the first situation and a decrease of 41% for the second one. A similar trend is observed for θ = 45°, although the differences are less important. As the permeability of the porous medium Da is increased, the boundary frictional resistance becomes gradually more important and adds to the bulk frictional drag induced by the solid matrix to slow down the convection motion. As a result, the effects of varying the anisotropy of the porous medium become less and less important. Also, the value of the heat transfer within the cavity drops significantly. When Da is high enough; i.e., when the resistance resulting from the boundary effects is predominant with respect to that due to the solid matrix, the present solution approaches that for a pure viscous fluid, Equation 40, and this independently of the anisotropy of the porous medium. This situation is reached when $Da \simeq 10$ for the conditions of Figure 6.

Another view of the effect of varying Da on the heat transfer is depicted in Figure 7 where a correlation of Nu as a function of Da is presented for R = 500 and 1000 and $K^* = 0.25$ and 4. The Nusselt number predicted by Brinkman's model starts to deviate from Darcy's model at $Da \simeq 10^{-6}$, when the convective motion is relatively high ($R = 10^3$, $K^* = 0.25$), and $Da \simeq 10^{-5}$ when it is relatively low ($R = 5 \times 10^2$, $K^* = 4$). The pure viscous fluid situation is represented in Figure 7 by dotted lines. This situation is reached at approximately $Da \simeq 2$ when $R = 5 \times 10^2$ and $Da \simeq 0.5$ for $R = 10^3$. For intermediate values of the Darcy number, it is seen that, as expected, the anisotropic effects of the porous medium become more important as the Rayleigh number is made larger.

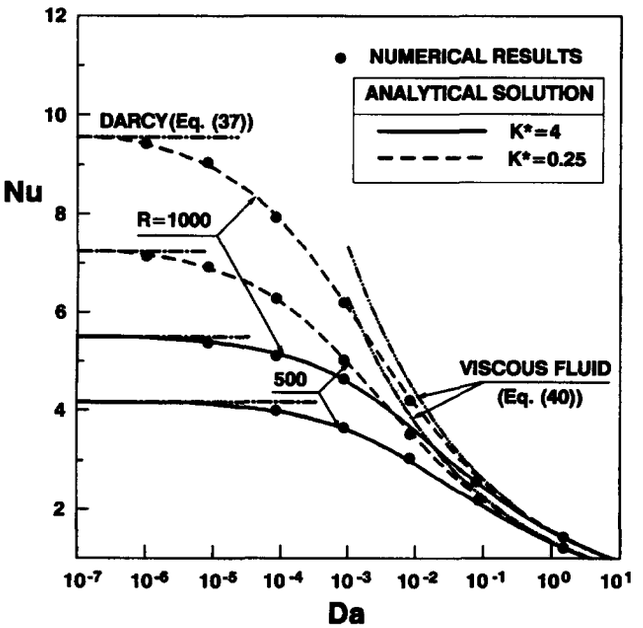

Figure 7 Effect of the Darcy number on Nusselt number for R=500 and 1000, θ=45°, and K^*=0.25 and 4

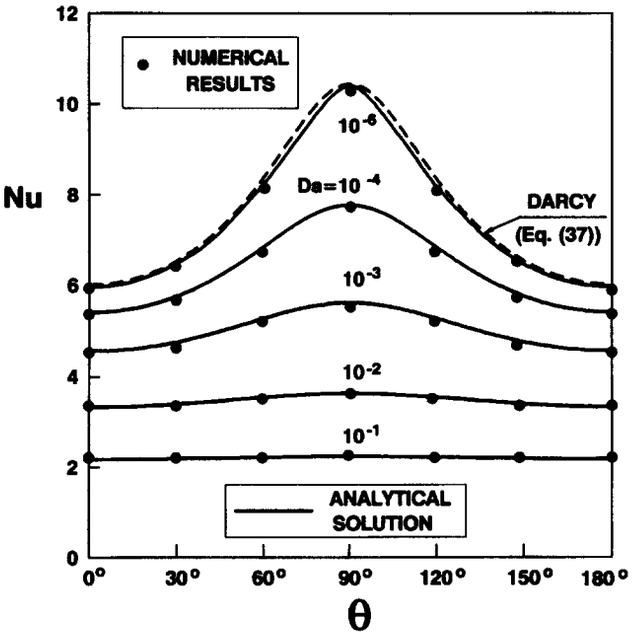

Figure 8 Effect of the inclination angle θ on Nusselt number for R=500, $K^*=0.25$, and various values Da

Figure 8 shows the effects of varying the Darcy number Da and anisotropic orientation θ on the Nusselt number for R = 500 and $K^* = 0.25$. As expected, when the Darcy number is small enough ($Da \lesssim 10^{-6}$), both the numerical and analytical solutions are in agreement with Darcy's law (Equation 37) represented by a dashed line on the graph. In this limit, the heat transfer varies considerably with the angle θ. The heat transfer is observed to be maximum (minimum) at θ = 90° (0° and 180°), in agreement with the variation of the strength of the convective flow with θ discussed in Figure 4a. Upon increasing the permeability of the porous medium (i.e. Da) it is seen that, for the reason explained earlier, the heat transfer drops progressively and becomes less and less affected by θ. For example, the case with $Da = 10^{-1}$ corresponds to a pure fluide situation for which Nu = (2.25), in agreement with Equation 40, independently of θ.

Conclusions

The problem of a vertical rectangular porous cavity, subject to constant heat fluxes applied on the side walls, has been investigated. The porous medium is assumed to be hydrodynamically anisotropic, with the principal axes of anisotropic permeability inclined with respect to the gravity force. The Brinkman-extended Darcy model, which allows the no-slip boundary condition to be satisfied, is used in the formulation. An analytical solution, valid in the boundary-layer regime, is derived on the basis of the modified Oseen technique. A finite-difference procedure is also developed to assess the validity of the analytical results. A good agreement between the boundary-layer solution and numerical simulations is obtained in the range of the governing parameters considered in this study. The following conclusions are drawn.

(1) When Da is small enough (low-porosity media), the flow field resembles that given by a pure Darcy analysis. For this situation, which holds for $Da \lesssim 10^{-6}$, the viscous effects near the boundaries are negligible, and both the permeability ratio and inclination of the principal axes of anisotropic permeability have a strong influence on the convection heat transfer.

(2) For intermediate values of Da, the boundary frictional resistance becomes gradually more important, as Da is increased, and adds to the bulk frictional drag induced by the solid matrix to slow down the convection motion. As a result, the effects of the anisotropic permeability of the porous medium on the convection heat transfer are progressively inhibited.

(3) When Da is large enough ($Da \gtrsim 10$), the present solution, based on the Brinkman-extended Darcy model, approaches that of a pure fluid medium (in the absence of inertia effects).

Acknowledgments

This work was supported in part by the National Sciences and Engineering Research Council, Canada and jointly by the FCAR, Government of Quebec.

References

Aboubi, K., Robillard, L. and Bilgen, E. 1995. Natural convection in horizontal annulus filled with an anisotropic porous medium. *ASME/JSME Thermal Eng. Conf.* **3**, 415–422

Bejan, A. 1983. The boundary-layer regime in a porous layer with uniform heat flux from the side. *Int. J. Heat Mass Transfer*, **26**, 1339–1346

Castinel, G. and Combarnous, M. 1974. Critère d'appariton de la convection naturelle dans une couche poreuse anisotrope. *C. R. Hebd. Seanc. Acad. Sci. Paris B*, **B278**, 701–704

Chan, B. K. C., Ivy, C. M. and Barry, J. M. 1970. Natural convection in enclosed porous media with rectangular boundaries. *J. Heat Transfer*, **92**, 21–27

Cheng, P. 1978. Heat transfer in geothermal systems. *Adv. Heat Transfer*, **14**, 1–105

Degan, G., Vasseur, P. and Bilgen, E. 1995. Convective heat transfer in a vertical anisotropic porous layer. *Int. J. Heat Mass Transfer*, **38**, 1975–1987

Degan, G. and Vasseur, P. 1996. Natural convection in a vertical slot filled with an anisotropic porous medium with oblique principal axes. *Numer. Heat Transfer*, Part A, **30** 397–412

Epherre, J. F. 1975. Critère d'apparition de la convection naturelle dans une couche poreuse anisotrope. *Rev. Gen. Thermique*, **168**, 949–950

Kimura, S. and Bejan, A. 1984. The boundary-layer natural convection regime in a rectangular cavity with uniform heat flux from the side. *J. Heat Transfer*, **106**, 98–103

Kimura, S., Masuda, Y. and Kazuo Hayashi, T. 1993. Natural convection in an anisotropic porous medium heated from the side (effects of anisotropic properties of porous matrix). *Heat Transfer Japan. Res.*, **22**, 139–153

Kvernvold, O. and Tyvand, P. A. 1979. Nonlinear thermal convection in anisotropic porous media. *J. Fluid Mech.*, **90**, 609–624

Ni, J. and Beckermann, C. 1991. Natural convection in a vertical enclosure filled with anisotropic porous media. *J. Heat Transfer*, **113**, 1033–1037

Nield, D. A. and Bejan, A. 1992. *Convection in Porous Media*, Springer-Verlag, New York

Nilsen, T. and Storesletten, L. 1990. An analytical study on natural convection isotropic and anisotropic porous channels. *J. Heat Transfer*, **112**, 396–401

Tong, T. W. and Subramanian, E. 1985. A boundary-layer analysis for natural convection in vertical porous enclosure-use of the Brinkman-extended Darcy model. *Int. J. Heat Mass Transfer*, **28**, 563–571

Tyvand, P. A. and Storesletten, L. 1991. Onset of convection in an anisotropic porous medium with oblique principal axes. *J. Fluid Mech.*, **226**, 371–382

Vasseur, P. and Robillard, L. 1987. The Brinkman model for boundary-layer regime in a rectangular cavity with uniform heat flux from the side. *Int. J. Heat Mass Transfer*, **30**, 717–727

Vasseur, P., Satish, M. G. and Robillard, L. 1987. Natural convection in a thin, inclined porous layer exposed to a constant heat flux. *Int. J. Heat Mass Transfer*, **30**, 537–539

Zhang, X. 1993. Convective heat transfer in a vertical porous layer with anisotropic permeability. *Proc. 14th Canadian Congress of Applied Mechanics*, **2**, 579–580

Zhang, X., Nguyen, T. H. and Kahawita, R. 1993. Convection flow and heat transfer in an anisotropic porous layer with principal axes non-coincident with the gravity vector. *Proc. ASME Winter Annual Meeting, Fundamentals of Natural Convection* (New Orleans, LA), HTD, Vol. 264, ASME, New York, 79–86